Supplementary Information for "Filtering input fluctuations in intensity and in time underlies stochastic transcriptional pulses without feedback" by Sassi et al

Supplementary Information A: The single-cell experimental dataset

All the experimental data analyzed in this paper are from the published single cell experiments by Kim et al [19]. Briefly, to vary the class-1 expression strength, different constitutive artificial promoters are used to replace the native class-1 promoter (*flhDp*) and either T7 or mut4 sequence are used as the downstream ribosome binding site (RBS-1). The ratio of the effective number of class-1 proteins and fluorescent proteins produced is different for the mut4 and T7 strains. To account for this difference, we multiply the C_1 values by a factor (~ 0.22) for the strains with mut4 as RBS-1 (see SI in [19] for details).

The experimental dataset consists of ~ 100 independent single-cell time series for each class-1 promoter strain, each lasting for ~ 70 generations. The time interval between two consecutive time frames is 5 minutes. Given that the average division time is ~ 40 minutes, each time series has $\sim 70 \times 40/5 = 560$ time points on average, and there are on average $\sim 100 \times 560 = 56,000$ data points for each strain. In the main text of this paper, we consider three of the seven strains studied in [19]: $P1$, $P4$ and $P7$ (we use the same strain names as in [19]). These three strains are chosen to cover the full range ($\sim$ 20-fold) of class-1 promoter strength change in [19] .

Performing an additional derivative for the class-2 output inevitably adds noise to the fitting process. This is true in particular if the derivation is performed *directly* on the total fluorescence $F_2 = sC_2$, where s is the cell size and C_2 is the fluorescence density (assumed to be proportional to the protein concentration):

$$A_2^* = \frac{1}{s}\frac{dF_2}{dt}\,. \tag{A1}$$

One possible way to reduce the noise is to calculate the activity using derivatives of the concentration rather than the total fluorescence:

$$A_2 = \alpha C_2 + \frac{dC_2}{dt}\,. \tag{A2}$$

where $\alpha = \frac{1}{s}\frac{ds}{dt}$ is assumed to be constant in first approximation and is obtained by means of an exponential fit of the cell area during single cell cycles. The use of C_2 also has the advantage that the time series do not have discontinuities at cell division.

We can compare the fluorescence density C_2 and the activity calculated in two ways as shown in Fig. S1 (top and middle). We can see that the activity calculated using Eq. A2 reduces the noise significantly.

The gray area in Fig. S1 (top and middle) indicates the time interval in which the class-2 promoter is activated, leading to a non-zero fluorescence rate. We can see that the concentration does not match accurately the time interval of promoter activation.

All details of the experimental design and pre-processing of the noisy data can be found in [19].

Supplementary Information B: Distribution of class-1 concentration and multiplicative noise

In order to model the class-1 protein concentration we used a linear multiplicative noise in Eq. 2 in the main text rather than an additive noise. This choice is motivated by the form of the probability distribution. We can consider for example the class-1 distribution when the promoter strength is $P4$ (green data points in Fig. S2(A)). In case of additive noise, the concentration follows an Ornstein-Uhlenbeck process (OU) whose steady state distribution is Gaussian. In Fig. S2(A), we plot a Gaussian distribution (black curve) with the same mean and variance as the experimental data as well as the distribution (red curve) obtained with a multiplicative noise. Fig. S2(A) clearly shows that the fluctuations in C_1 are better described by a stochastic model (Eq. 2 in the main text) with a multiplicative noise. Another choice of multiplicative noise is to multiply the noise by $\sqrt{C_1}$ instead of C_1. We also tested this square-root noise by running simulations using the parameters that are needed to obtain the same mean value and variance as in the experiment for the case of promoter P4. While the distribution of A_2 from the square-root noise model fits the data better than the additive noise (blue curve), it is not as good as our model with linear multiplicative noise. Quantitatively, if we compare the cumulative distributions (Fig. S2(B)) by using the Kolmogorov-Smirnov test, the maximal deviation (with respect to the experimental curve) is 2.56% in the case of linear noise versus 3.79% in the case of square root noise.

Supplementary Information C: Model parameters and response functions determined by fitting model to the single-cell experimental dataset

In this paper, we develop a simple stochastic model with a minimal set of biologically meaningful parameters and response functions, which can be determined by fitting our model to the large experimental data set described in Sec. A.

For the C_1 dynamics described in Eq. 2 in the main text, there are three parameters: the timescale τ_1, the multiplicative noise strength Δ_1, and the promoter strength μ, which is different for different strains. In our study, τ_1 can be set to unity to set the timescale of the problem, all other timescales are scaled by τ_1. By fitting our model to the experimental data, we found that the noise strength $\Delta_1 \approx 0.1\tau_1^{-1}$, and the promoter strength for different strains are: $\mu(P1) = 2.6$, $\mu(P4) = 13.7$, $\mu(P7) = 44.7$, in the unit of florescence intensity.

The dynamics of class-2 activity A_2 is determined by a timescale τ_2, the response function $f_s(C_1)$, and a noise strength Δ_s that is different for different strains. The parameters and response functions are obtained by fitting our model to the experimental data (class-2 activity dynamics). The range of τ_2/τ_1 is determined as shown in Fig. 2 in the main text. The noise strength Δ_+ and Δ_- for different strains in the presence and absence of YdiV are also determined and their values are shown in Fig. S3.

For the response functions we used the Hill curves of the form

$$f_s(C_1) = d_0 + (d_1 - d_0)\frac{C_1^{H_s}}{C_1^{H_s} + K_{1/2,s}^{H_s}}\,, \tag{C1}$$

where constrained the parameters d_0 and d_1 to have the same value in the presence and the absence of YdiV, because the theory suggests that the value of the lower and upper plateau should not depend on YdiV. We then tuned (searched) these parameters (d_0,d_1, $K_{1/2,\pm}$, $H_\pm$) within a range such that the mean values of C_1 and A_2 for different promoters never deviate more than 10% from the experimental values, and we then selected the values for the parameters that minimize the deviation of the model distributions from the experimental distribution of $A_2/\langle A_2\rangle$. As a result, the following values were obtained: $d_0 = 0.09$, $d_1 = 46$, $K_{1/2,+} = 25$, $K_{1/2,-} = 22$, $H_+ = 12$, $H_- = 3$.

In Fig. S4, we show the average C_1 versus average A_2 for a single cell over many generations from experiments and model. The response functions are also shown (the same as in Fig. 1D in the main text).

Supplementary Information D: Testing the model in strains with different promoter strengths

To test the self-consistency of our model for all experimentally studied strains, we ran simulations of our model using promoter strengths $P2$ and $P5$, which were not used to determine the model parameters and the response function reported in the main part of this paper. We found that the experimentally observed A_2 statistics can be successfully reproduced by using $\mu(P2) = 6.1$ and $\mu(P5) = 21.9$ while keeping all other model parameters and the response function the same as those determined from the strains ($P1, P4, P7$), which were used to calibrate our model. As shown in Fig. S5, there is a shift in the peak of the distribution of the normalized activity A_2 toward low values for $P5$. This is due to the fact that the promoter strength of the $P5$ promoter is close to the region of maximal steepness in the response curve, as we can see from Fig. S4, in which the response curves are shown together with the mean values of C_1 and A_2 for simulations and experiments. This effect is present but less pronounced for $P2$, which has a promoter strength that is in the region of the lower plateau in the response function.

Supplementary Information E: Comparison of model and experiments in strains with different YdiV levels

As $K_{1/2}$ in the response function increases with the YdiV level, the effect of increasing YdiV level is captured in our model by varying $K_{1/2}$ (increasing the Hill coefficient further from its already high value does not have a significant effect). As expected, our simulations show that as $K_{1/2}$ increases the class-2 gene expression level distribution shifts towards lower values (Fig. S6A). To compare with the population-level gene expression distribution from flow cytometry experiments (see below), we computed the class-2 gene expression level C_2 by integrating the class-2 activity A_2 over a time window corresponding to the average division time $T \approx 45min$: $C_2(t) = \int_t^{t+T} A_2(t')dt'$. The blue curves in Fig. S6 correspond to the WT cells with $K_{1/2} = 25$ determined from our modeling study.

The strains used for the experiments have the native YdiV knockout and contain a plasmid in which YdiV is controlled either by ProB or ProD constitutive promoter [36]. They also have the same reporting system as in the other strains used in this work [19]: CFP expres-

sion is controlled by the class-2 promoter fliFp, and YFP by the class-1 promoter regulator *flhDp*. The list strains are: WT: MGR-E98K, galK::AmpR-PfliF-CFP, attB::KmR-PfliF-YFP; ProB_YdiV: MGR-E98K, galK::AmpR-PfliF-CFP, attB::KmR-PfliF-YFP, ydiV::FRT, pProB_YdiV; ProD_YdiV: MGR-E98K, galK::AmpR-PfliF-CFP, attB::KmR-PfliF-YFP, ydiV::FRT, pProD_YdiV. List Plasmids: pProB_YdiV : Plasmid SC101 origin, GentR, ProB::YdiV; pProD_YdiV : Plasmid SC101 origin, GentR, ProD::YdiV.

Cells were grown in a flask with liquid rich defined media at 30 °C until they reached exponential growth and then measured using flow cytometry. As in the microfluidic experiments, the growth media used was a modified version of Neidhardt EZ–rich medium (Teknova), with the 0.2% glucose being replaced with 0.4% glycerol to prevent catabolite repression of flagellar synthesis.

Fig. S6 shows that the distributions from the flow cytometry experiments have the same shape and more importantly the same general dependence on YdiV level as those from our model.

Supplementary Information F: Estimating the timescale ratio

The separation of timescales seems to be independent of the presence or absence of YdiV. In Fig. S7, we show the BARC's from experimental data for strains with YdiV and those from our model, which are similar to the results for strains without YdiV (Fig. 2 in the main text). Quantitatively, BARCs can be used to estimate the timescale ratio τ_2/τ_1. To quantify the shape of BARC, we define a flatness parameter as the absolute value of the inverse of the average slope of linear fits to BARC's of different strains such as those shown in Fig. 2 in the main text and Fig. S7 here. A larger flatness means that the class-2 activity has a stronger dependence on the average FlhDC level than its instantaneous value and thus the memory effect is stronger. We computed the flatness for different values of the relative timescale ratio τ_2/τ_1 in our model. As shown in Fig. S8, a larger τ_2/τ_1 ratio leads to a larger flatness, i.e., a stronger memory effect. Based on a quantitative comparison with the flatness values obtained from experimental data with and without YdiV, we estimate the ratio τ_2/τ_1 to be in the interval, $2.1 \leq \tau_2/\tau_1 \leq 3.6$, shown as the gray region in Fig. S8. In addition, in Fig. S9, we compare the autocorrelation function for wild type cells shown in [19] with the autocorrelation functions obtained from the simulations of our model (Eq. 1 and 1). The

difference in the timescales between class-1 and class-2 is in line with the interval estimated by the analysis of the flatness shown in Fig. S8.

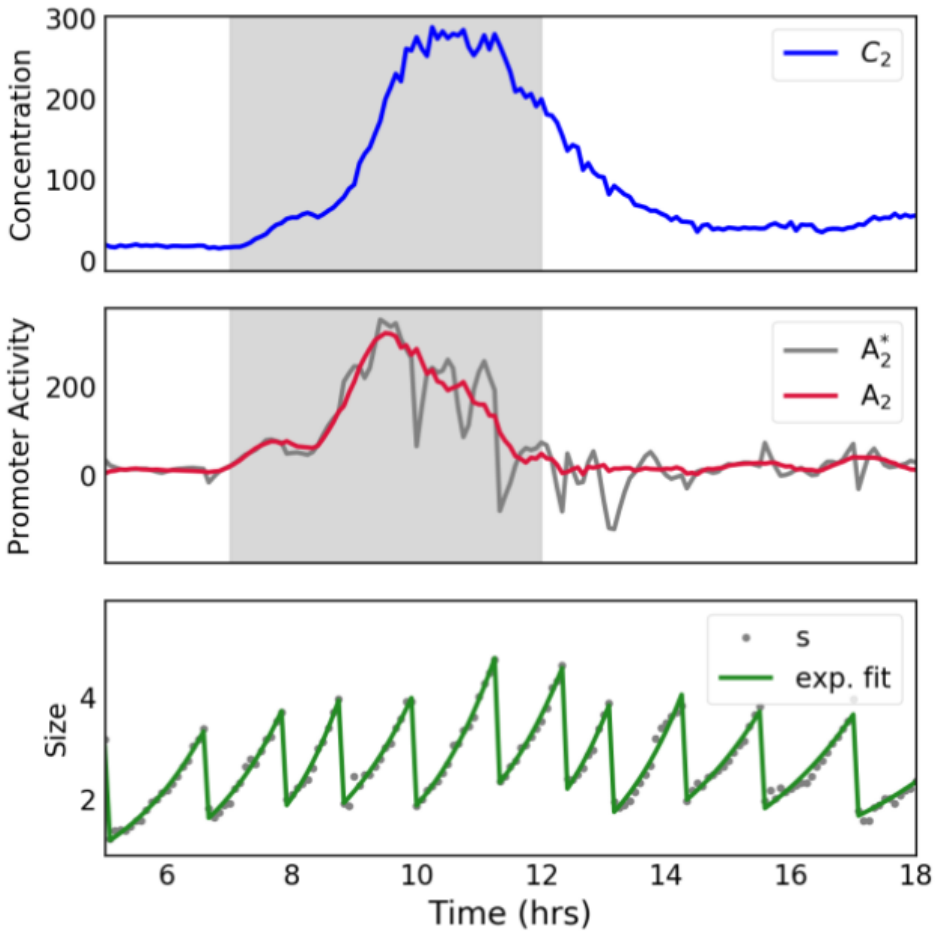

FIG. S1: (top) Class-2 concentration as a function of time. (middle) Activity calculated in two different ways as a function of time. (bottom) Time traces of the cell size. Figure based on Kim *et al.*, Fig. S11.

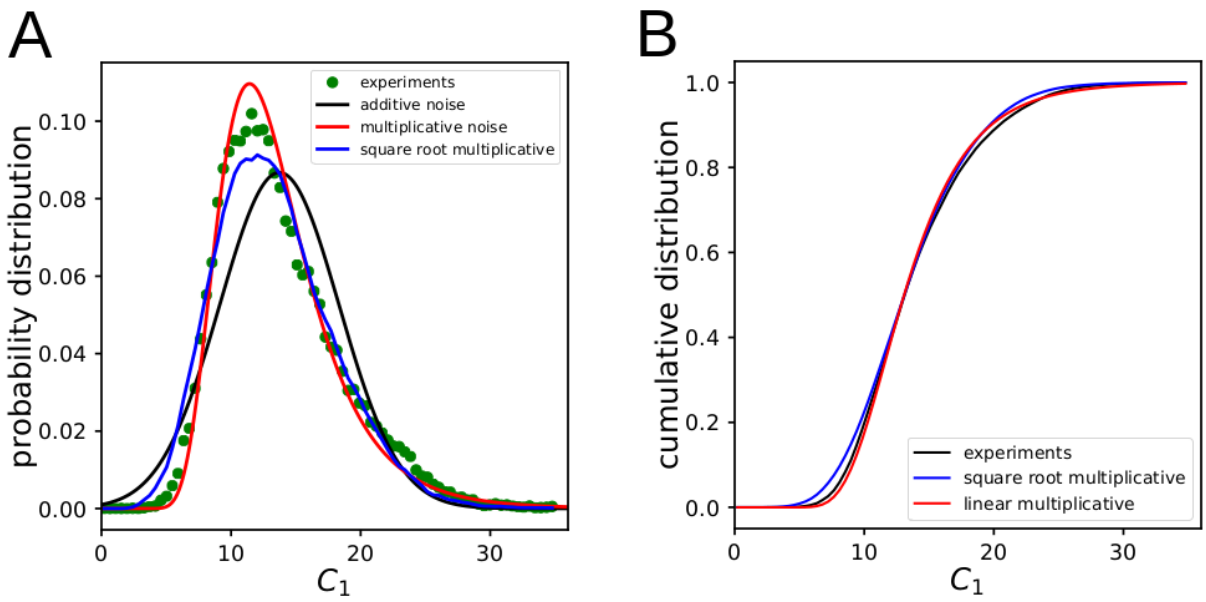

FIG. S2: (A) Comparison of the C_1 distributions from our model with different forms of noise with experimental data for the $P4$ strain. Both forms of multiplicative noise (linear and square root) lead to much better fit with the data than the additive noise. (B) Cumulative distribution for C_1 in the cases of linear (red) and square root (blue) multiplicative noise, together with the experimental results (black). The Kolmogorov-Smirnov test shows that the linear multiplicative noise leads to a smaller error (2.56%) than that for the square-root noise (3.79 %).

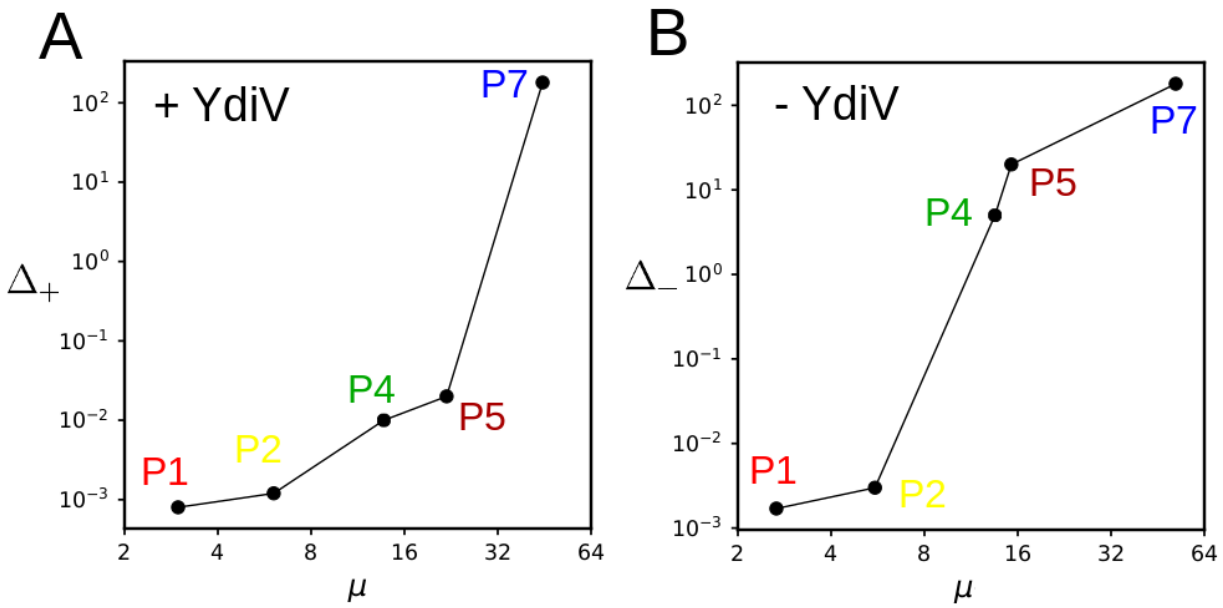

FIG. S3: Noise strength $\Delta_{+,-}$ (in the presence and absence of YdiV) as a function of the average class-1 protein level $\langle C_1 \rangle$ obtained by fitting the stochastic model (Eq. (1-2) in the main text) to experimental data.

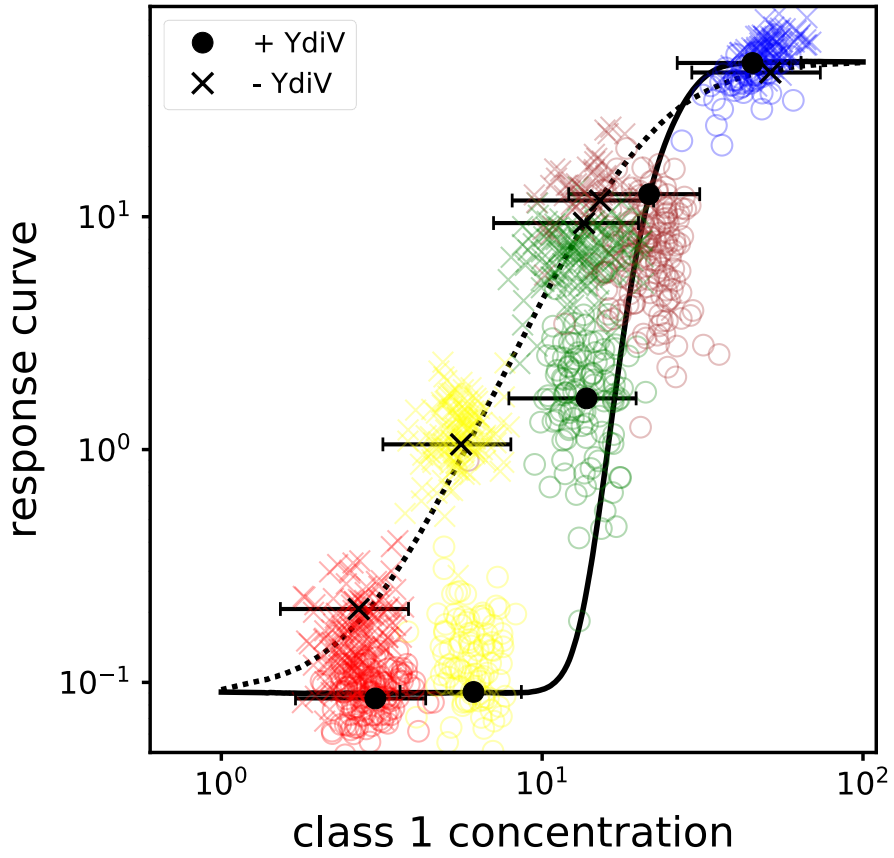

FIG. S4: Response functions $f_{+,-}(C_1)$ used in the model, in the presence (solid) and absence (dashed) of YdiV. The black circles and crosses indicate the mean value obtained with the stochastic model. The horizontal error bars (for C_1) are given by $\sigma = \langle C_1 \rangle \sqrt{2\Delta_1}$, where Δ_1 is the strength of the noise η for class-1 protein level.

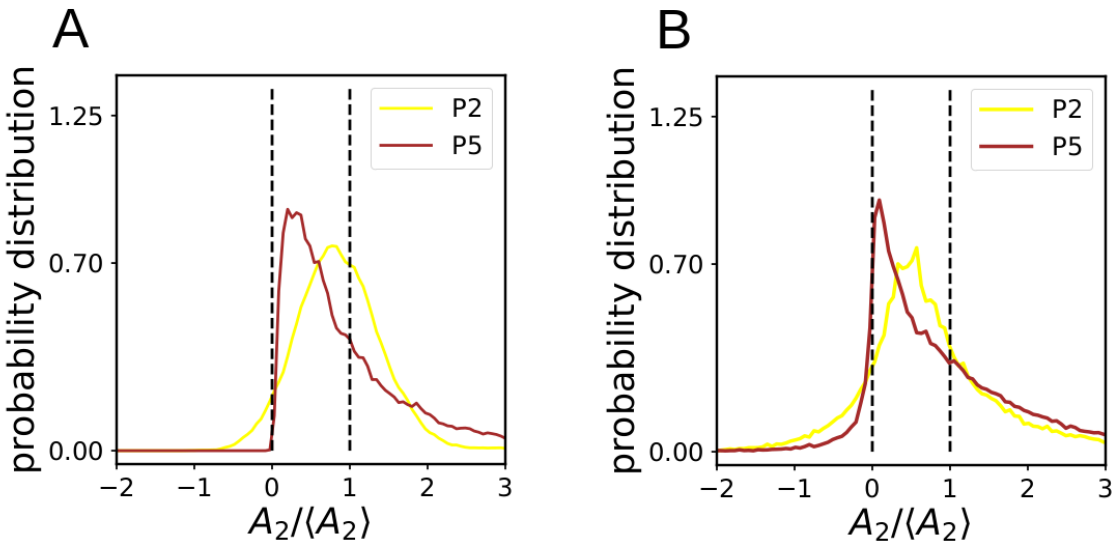

FIG. S5: Distributions of normalized A_2 from model simulations (A) and experiments (B) for strains $P2$ and $P5$.

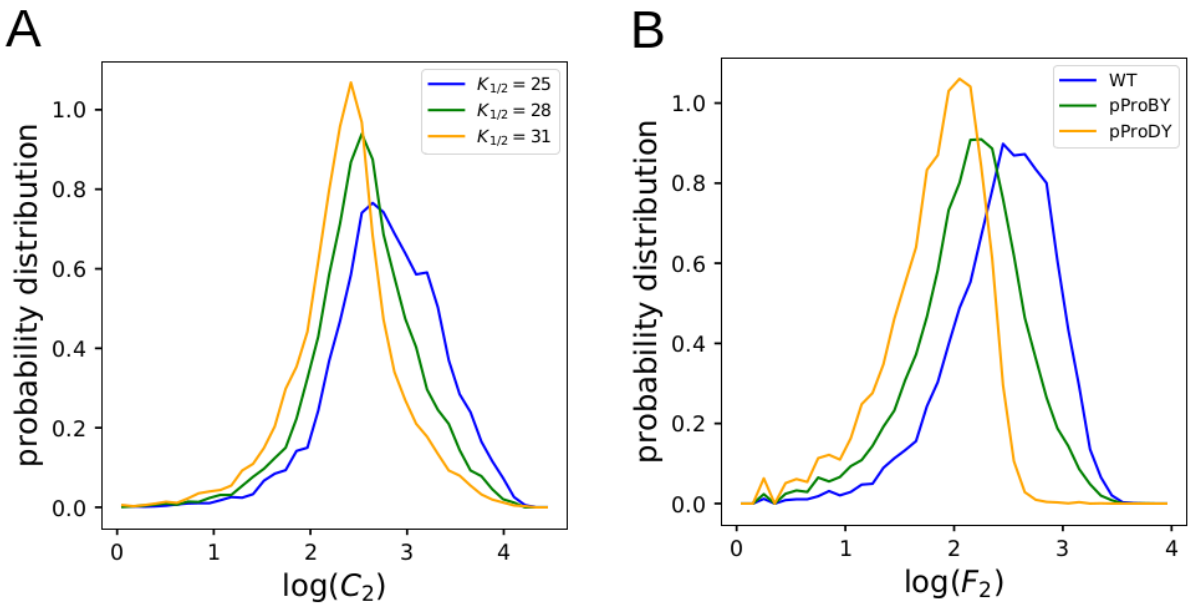

FIG. S6: (A) Distributions of the logarithm of C_2 for different $K_{1/2}$ values from our model. (B) Distributions of the logarithm of the fluorescence (F_2) from the flow cytometry measurements for different strains with different YdiV levels. The orange distributions represent the case with a high (saturating) level of YdiV where class-2 gene has minimal activity. In our model, this corresponds to the situation with a large enough $K_{1/2}$ such that the range of C_1 levels fall almost entirely in the lower plateau of the response function.

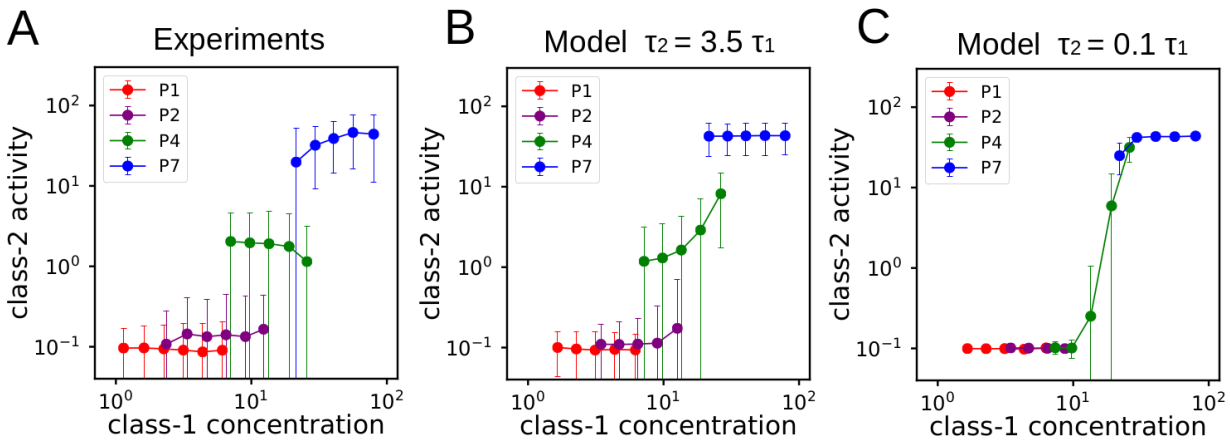

FIG. S7: The bin-averaged response curves and the ratio of two timescales τ_2/τ_1. (A) The bin-averaged response curves with different class-1 promoter strength from experimental data [19] for strains with YdiV. Different colors are used for different class-1 promoters. The corresponding model results for (B) $\tau_2 = 3.5\tau_1$ and (C) $\tau_2 = 0.1\tau_1$.

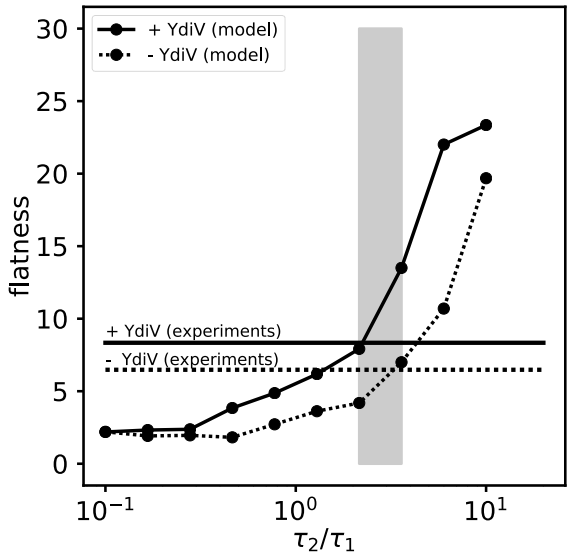

FIG. S8: The estimated range of the timescale ratio τ_2/τ_1. Flatness of the bin-averaged response curves as a function of τ_2/τ_1 in the absence (dashed line) and presence (solid line) of YdiV. The horizontal lines indicate the experimental results. Comparing the model results with the experiments, we estimate the ratio τ_2/τ_1 to be within the gray region: $2.1 \leq \tau_2/\tau_1 \leq 3.6$.

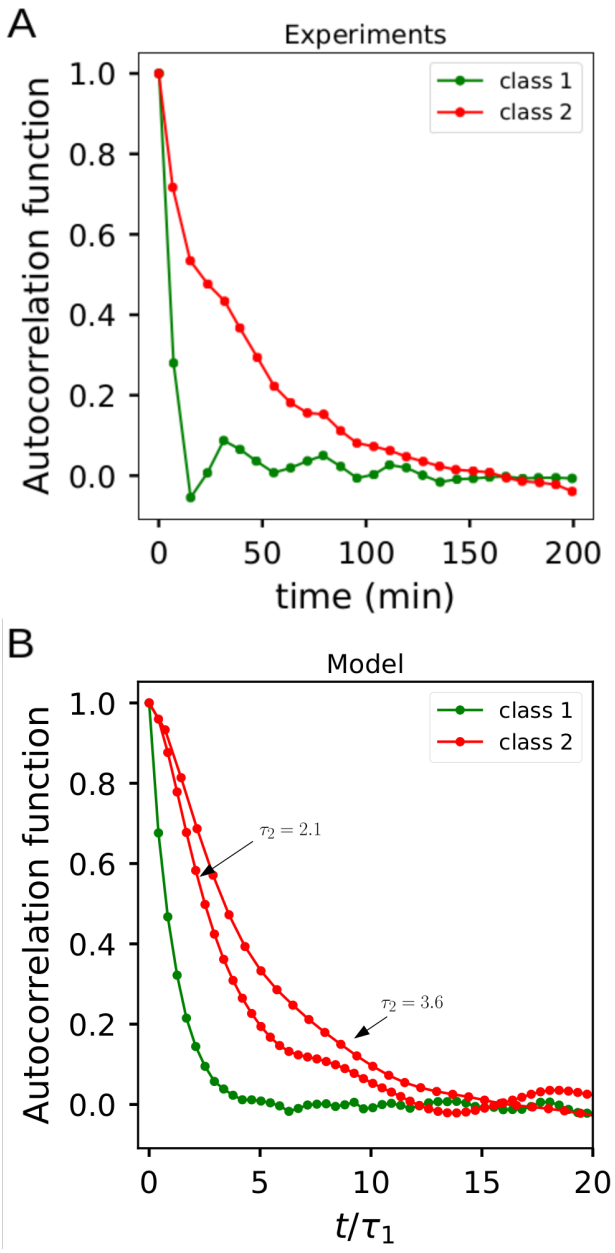

FIG. S9: (A) Autocorrelation functions for the fluorescence of class-1 and class-2 reporters in the case of wild type promoters (taken from Fig. 2D in [19]). (B) Autocorrelation functions for C_1 and A_2 from the stochastic simulations of our model (Eq.1 and Eq.2) for $P4$ strain.

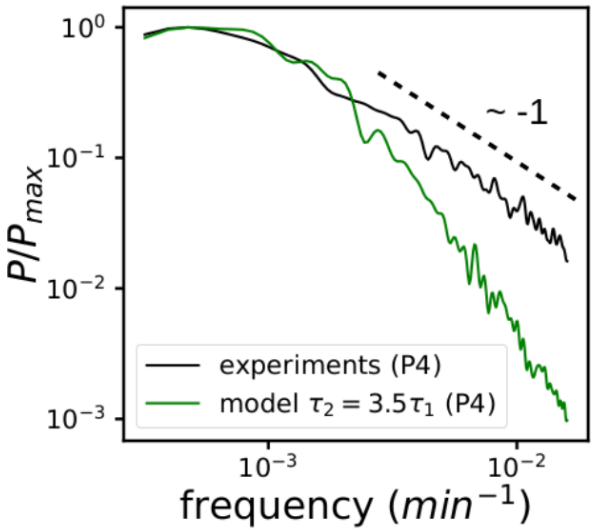

FIG. S10: The power spectrum in log-log scale. The power spectrum from experimental data agrees with our model in the low frequency regime. In the high frequency regime, it decays as f^{-1} slower than the model result. This $1/f$ noise may be caused by fluctuations of YdiV level, which can introduce a spectrum of timescales to the system.